Solid State Sciences 157 (2024) 107699

Contents lists available at ScienceDirect

Solid State Sciences

journal homepage: www.elsevier.com/locate/ssscie

# Production, structure and magnetic properties of nanocomposites based on the perovskite phase $LaFeO_3$

O.V. Chudinovych [a,b,*], D.V. Vedel [a], O.O. Stasyuk [c], T.V. Tomila [a], M.H. Aguirre [d,e,f]

[a] I. M. Frantsevich Institute for Problems in Materials Science NAS of Ukraine, 3, Omeliana Pritsaka St., 03142, Kyiv, Ukraine
[b] National Technical University of Ukraine «Igor Sikorsky Kyiv Polytechnic Institute», 37, Peremohy Ave., 03056, Kyiv, Ukraine
[c] G. V. Kurdyumov Institute for Metal Physics of the NAS of Ukraine, 36, Akademika Vernadskyi Boulev., 02000, Kyiv, Ukraine
[d] Institute of Nanoscience and Materials of Aragon, University of Zaragoza-CSIC, Mariano Esquillor s/n, 50018, Zaragoza, Spain
[e] Dept of Physics Condensed Matter, University of Zaragoza, Pedro Cerbuna 12, 50018, Zaragoza, Spain
[f] Laboratory of Advanced Microscopy, University of Zaragoza, Mariano Esquillor s/n, 50018, Zaragoza, Spain

ARTICLE INFO

*Keywords:*
Nanopowders
Iron oxide
Lanthanum oxide
Perovskite-type phase
Magnetic properties

ABSTRACT

The phase relations in the $La_2O_3$–$Fe_2O_3$ system at 1300 °C were studied in the whole concentration range by X-ray diffraction (XRD) and scanning electron microscopy (SEM). The samples were prepared with a concentration step of 1–5 mol %. The isothermal cross-sections of the $La_2O_3$–$Fe_2O_3$ phase diagram at 1300 °C are characterized by the presence of three single-phase (A–$La_2O_3$, $LaFeO_3$, $Fe_2O_3$), two two-phase (A–$La_2O_3$+$LaFeO_3$, $LaFeO_3$+$Fe_2O_3$) regions. The composition corresponding to the perovskite phase is 49 mol % $La_2O_3$–51 mol % $Fe_2O_3$. Nanocomposites based on the perovskite phase ($LaFeO_3$) were obtained by the Pechini method and heterogeneous precipitation from nitrate solutions. Solutions of $La^{3+}$ nitrates, which were obtained by dissolving lanthanum oxide with a content of the main component of 99.99 % in nitric acid. The influence of the production method on the microstructure, morphology, and magnetic properties of nanopowders ($LaFeO_3$) was studied. According to XRD, infrared spectroscopy, SEM, and TEM, the synthesized perovskite $LaFeO_3$ is single-phase with a particle size of 50–60 nm. The morphology of powder particles primarily depends on the method of material synthesis. The powder showed ferrimagnetic magnetic properties and had a specific magnetization 0.2 and 0.15 emu/g.

## 1. Introduction

The need for new materials is increasing due to the development of existing and new branches of technology. Rare earth elements play a significant role in creating new materials. Oxides of rare earth elements (REE) are promising for the creation of materials for a wide range of use in radio electronics, optoelectronics, instrument engineering, nuclear and laser technology, mechanical engineering, chemical industry, metallurgy, medicine, etc. [1–9]. Today, it is important to create new materials with high magnetic properties. As of 2022, the four most common types of magnets are produced in the world: soft (20 % of the market), semi-hard (60 % of the market), permanent (10 % of the market), and special-purpose magnets (10 % of the market) [10]. Ferrites are of particular interest as they have a relatively low price with fairly high magnetic properties that can be improved by doping. There is great practical interest in intermediate phases based on REE with a perovskite-type structure. Perovskite-type oxides have a chemical formula of $RBO_3$ (R = rare earth metals, B = transition metals). These materials have become some of the most promising candidates for ferroelectricity, piezoelectricity, pyroelectricity, high-temperature superconductivity, magnetic behavior, and catalytic activity due to their wide unique physical and chemical properties. These properties determine the use of such materials in many applications such as gas transducers, catalysts, solid electrolyte batteries and magnetic sensors [11]. Among perovskite-type oxides, $LaFeO_3$ is of interest because of its low price, non-toxicity, abundant reserve, and excellent electrochemical capacity [11]. Doping $Fe_2O_3$ with rare earth elements has a great influence on the magnetic properties of the obtained materials [12]. Chemical compounds of iron oxide $Fe_2O_3$ doped with oxides of rare earth metals $Ln_2O_3$ possess special magnetic (ferromagnetic) properties with high magnetization ($H_c(PrFeO_3) = 505.45$ Oe; $H_c(HoFeO_3) = 2659$ Oe; $H_c(YFeO_3) = 53.36$ Oe) [23]. Due to these properties, they have

* Corresponding author. I. M. Frantsevich Institute for Problems in Materials Science NAS of Ukraine, 3, Omeliana Pritsaka St., 03142, Kyiv, Ukraine.
*E-mail addresses:* chudinovych_olia@ukr.net, o.chudinovych@ipms.kyiv.ua (O.V. Chudinovych).

https://doi.org/10.1016/j.solidstatesciences.2024.107699
Received 19 July 2024; Received in revised form 31 August 2024; Accepted 10 September 2024
Available online 13 September 2024

found wide applications as magnetic materials in radio engineering, radio electronics, computer engineering, catalysis, gas-separation fuel cells, magneto-optical devices, electromagnetic equipment, environmental monitoring, modern information storage with spin valves, etc [13].

The magnetic structure of $RFeO_3$ is formed by Fe and R sublattices, which simultaneously contain 3d and 4f electrons. The magnetic interaction is an antiferromagnetic interaction that is responsible for the high Néel temperatures (TN) in the range of 620–740 K for these types of compounds. Since the $R^{3+}$ sublattices are nonmagnetic, their magnetization (with moment m) is acquired due to the interaction with the $Fe^{3+}$ sublattices, which causes polarization of $R^{3+}$ cations as quasi-paramagnetism [13]. In recent years, rare-earth orthoferrites $RFeO_3$ have become the center of research for the development of multiferroics [14–23]. $LaFeO_3$ was prepared by various methods: sol-gel method [11], polymerized complex method [20], and hydrothermal method [15]. In Refs. [15–23] the properties of orthoferrates of lanthanides were obtained and studied but the chemical composition of the materials was not determined in these works. The right choice of optimal compositions for the synthesis of materials is the key to obtaining materials with the desired physical and chemical properties. The reference material for determining the optimal compositions is the state diagrams, as they can be used to determine the region of existence of solid solutions. Phase diagrams based on REE oxides, where perovskite-type phases are formed ($LnLn'O_3$ (Ln, Ln' = REE)) have been studied [24–26], and systems based on iron oxide and rare earth elements, in which a perovskite-type phase is also formed ($LnFeO_3$ (Ln = REE)) has not been fully investigated, the data contradict each other and require clarification [27,28]. This necessitates a systematic study of phase equilibria in this system and a determination of the composition that corresponds to the perovskite-type phase.

Despite the promising nature of these materials, existing research is unsystematic, which makes it necessary to expand and supplement the existing knowledge base about materials based on the $Fe_2O_3$-REE system and to achieve a deeper understanding of the relationship between the structure and magnetic properties of the material.

The purpose of this work is to obtain materials based on the $LaFeO_3$ perovskite phase and to study their magnetic properties and crystal structure.

## 2. Materials and methods

$La_2O_3$ (LaO-1 grade) with a content of the main component of 99.99 %, $Fe(NO_3)_3{\cdot}9H_2O$, ammonia, $NH_2CONH_2$ and nitric acid were used as starting materials.

Nanopowders based on the perovskite phase were obtained by the Pechini method ($LaFeO_3$(I)) and heterogeneous deposition ($LaFeO_3$(II)). The essence of the method Pechini is to achieve a high degree of cations mixing in the solution, the controlled transition of the solution into a polymer gel, the removal of the polymer matrix with the formation of an oxide precursor, and the preservation of a high degree of homogeneity. Solutions of $La^{3+}$ nitrates, which were obtained by dissolving lanthanum oxide with a content of the main component of 99.99 % in nitric acid, were used as starting materials. Before preparing the initial solutions, lanthanum oxide was pre-dried in a muffle at 300 °C for 2 h. A mixture with different $La^{3+}$ and $Fe^{3+}$ content was prepared from nitrate solutions. The mix of nitrate and citric acid solutions was stirred for 1 h at 80 °C. The obtained precursor was dried at 150 °C for 24 h and then subjected to heat treatment at 800 °C.

Synthesis of the precursor by the method of heterogeneous precipitation was carried out from a mixture of solutions of nitrates $La^{3+}$ and $Fe^{3+}$ at a concentration of 0.1 mol/l, the temperature of the solution during the precipitation of the mixture was 80 °C. As a precipitant, the 1 M ammonia solution with a urea of 5 vol % was used. The obtained sediment of the precursor was separated by triple centrifugation with distilled water and a single centrifugation in the presence of ethyl alcohol and dried at 120 °C for 24 h.

The determination of the characteristics of the samples was carried out using physicochemical methods X-ray diffraction (XRD), thermogravimetric analysis, electron microscopy (SEM, TEM) and IR spectroscopy.

For phase composition analysis, X-ray patterns were obtained on an X-ray diffractometer DRON-3M (CuKα-radiation with a nickel filter). The scan angle was 0.05–0.1° in the range 2θ = 15–80°. A DQ-1000 derevatograph was used for thermogravimetric analysis. The study of IR spectra was carried out using an FSM-1201 spectrometer in the wavelength range of 4000–400 $cm^{-1}$. For IR spectroscopic studies, the obtained samples were thoroughly mixed with KBr powder in the ratio (1:300) milligrams and the resulting mixture was pressed into transparent tablets 13 mm in diameter. Scanning electron microscopy (SEM) was used to assess the homogeneity of the powders. Elemental analysis of the samples was performed by X-ray spectral microanalysis (XMR) using an energy dispersive spectrometer (EDS) INCA 450 (OXFORD Instruments). Transmission Electron Microscopy (TEM) was performed by Tecnai F30 (FEI) working at 300 keV and with EDS in-situ spectroscopy. The atomic concentrations of the elements were determined within the relative experimental error of ~0.2 % for the investigated area of 500 μm × 500 μm. The specimens with dimensions 5 mm in diameter and 2 mm in height and powders were used to measure magnetic properties. A rigid cuvette measured the magnetic properties was also motivated by the fact that the vibrating sample magnetometer (LDJ-9500, LDJ Electronics, Troy, MI 48099, USA) used for magnetostatic measurements creates a working acceleration of 25gn, where gn is the standard gravity. The basic property of the magnetostatic measurements of the samples in the magnetic field range between −10 and + 10 kOe is that the M(H)-dependences were completely reproducible after repeated recording at room temperature. M denotes the magnetization of the composite material and H is the external magnetic field strength.

## 3. Results and discussion

### 3.1. Phase composition in $La_2O_3$–$Fe_2O_3$ system at 1300°C

The chemical and phase compositions in $La_2O_3$–$Fe_2O_3$ system annealed at 1300°C with lattice constant are summarized in Table 1. The results were used to plot the isothermal section of the $La_2O_3$–$Fe_2O_3$ phase diagram at 1300°C (Fig. 1). The isothermal cross-sections of the $La_2O_3$–$Fe_2O_3$ phase diagram at 1300 °C are characterized by the presence of three single-phase (A–$La_2O_3$, $LaFeO_3$, $Fe_2O_3$), two two-phase (A–$La_2O_3$+$LaFeO_3$, $LaFeO_3$+$Fe_2O_3$) regions.

There are $La_2O_3$, $Fe_2O_3$, and $LaFeO_3$ (R) phase in $La_2O_3$–$Fe_2O_3$ system of at 1300°C, according to SEM and XRD analyses, Figs. 2 and 3, respectively. Depending on the lanthanum oxide and iron oxide content, microstructural changes in the samples can be followed in Fig. 2. The R phase is light and the $Fe_2O_3$ phase is dark. Diffractograms of samples characterizing the phase fields present in the $La_2O_3$–$Fe_2O_3$ system at 1300 °C are presented in Fig. 3. $LaFeO_3$ does not form regions of homogeneity, Fig. 1, Table 1. A change the composition by 1 mol % leads to a shift from a single-phase region ($LaFeO_3$) to a two-phase region ($LaFeO_3$+$La_2O_3$ or $LaFeO_3$+ $Fe_2O_3$). The boundaries of the homogeneity range for the phases formed in the system were determined according to the data provided in Table 1. It should be noted that the $La_2O_3$ hydrated in the air atmosphere at room temperature. Therefore, on the XRD the peak of $La(OH)_3$ was observed, Fig. 3d and e. Nevertheless, since this applies only to A-$La_2O_3$ in the investigated system, the results obtained for $La(OH)_3$ can be attributed to A-$La_2O_3$.

Microstructures of composite close to $LaFeO_3$ showed at Fig. 4. The single phase ceramics was formed at 49 mol% $La_2O_3$ and 51 mol % $Fe_2O_3$ (Fig. 4, a). The lattice constant corresponds to theoretical one ($a$ = 5.566 nm, $b$ = 7.854 nm, $c$ = 5.553 nm). Increasing the amount of $Fe_2O_3$ led to formation it in the microstructure, Fig. 4 b, c. The matrix light phase consist of ~17 at% La and ~19 at% Fe that correspond to

**Table 1**
– Phase composition and lattice parameters of the phases in the $La_2O_3$–$Fe_2O_3$ system, annealed at 1300 °C for 300 h in air (XRD and SEM data).

| Chemical composition, mol % | | Phase composition | Parameters of elementary cells of phases at 1300 °C, nm ($a \pm 0.0002$) | | | | | | |
|---|---|---|---|---|---|---|---|---|---|
| $Fe_2O_3$ | $La_2O_3$ | | R | | | $Fe_2O_3$ | | $La(OH)_3$ | |
| | | | *a* | *b* | *c* | *a* | *c* | *a* | *c* |
| 100 | 0 | $Fe_2O_3$ | | | | 0.511 | 1.382 | | |
| 95 | 5 | $Fe_2O_3$+ R | | | | 0.502 | 1.375 | | |
| 90 | 10 | $Fe_2O_3$+ R | 0.552 | 0.785 | 0.555 | 0.501 | 1.377 | | |
| 85 | 15 | $Fe_2O_3$+ R | 0.555 | 0.783 | 0.556 | 0.500 | 1.377 | | |
| 55 | 45 | $Fe_2O_3$+ R | 0.554 | 0.783 | 0.555 | 0.500 | 1.380 | | |
| 51 | 49 | R | 0.554 | 0.784 | 0.553 | | | | |
| 50 | 50 | R + $La(OH)_3$ | 0.555 | 0.787 | 0.551 | | | | |
| 49 | 51 | R + $La(OH)_3$ | 0.553 | 0.784 | 0.555 | | | | |
| 45 | 55 | R + $La(OH)_3$ | 0.554 | 0.783 | 0.555 | | | 0.652 | 0.383 |
| 30 | 70 | R + $La(OH)_3$ | 0.554 | 0.784 | 0.555 | | | 0.651 | 0.384 |
| 5 | 95 | R + $La(OH)_3$ | 0.557 | 0.786 | 0.555 | | | 0.653 | 0.385 |
| 2 | 98 | R + $La(OH)_3$ | | | | | | 0.653 | 0.385 |
| 1 | 99 | R + $La(OH)_3$ | | | | | | 0.652 | 0.385 |
| 0,5 | 99.5 | R + $La(OH)_3$ | | | | | | 0.651 | 0.385 |
| 0 | 100 | $La(OH)_3$ | | | | | | 0.654 | 0.385 |

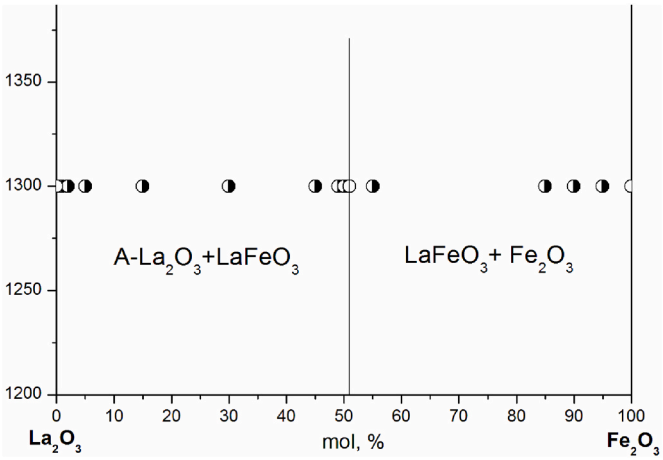


**Fig. 1.** - Isothermal section at 1300 °C for the system $La_2O_3$–$Fe_2O_3$ (○ – single-phase samples, ◐ - two-phase samples).

$LaFeO_3$ phase. Precipitation of dark phase has the chemical composition of ~42 at % of Fe with contamination of La in amount of ~0.6 at%. SEM and EDS results suggest that formation of two phase in 50 mol % $La_2O_3$–50 mol % $Fe_2O_3$ and 51 mol % $La_2O_3$–49 mol % $Fe_2O_3$ material, Fig. 4b and c, Table 2.

### 3.2. Thermogravimetric

The DTA curve of the precursor illustrates the presence of five minimums. Above 670°C, no thermal effects are recorded, and there is no mass loss of the sample. The endothermic peaks on the DTA curve in the low-temperature region are associated with the removal of adsorbed and structurally bound water and the decomposition of intermediate compounds. The intense effect recorded in the temperature range of 200–350 °C is due to the decomposition of the main compound, for the formation of which urea ($NH_2CONH_2$) was used (Fig. 5,b). The chemical activity of the $NH_2$ ligand contributes to the release of a large amount of energy during thermal decomposition. An intense endothermic effect in the temperature of 641 °C corresponds to the crystallization of the final product. Each effect of the DTA curve corresponds to the loss of mass on the TG curve. The total mass loss of the sample is ~70 % ($LaFeO_3$(I)) and ~36 % ($LaFeO_3$(II)). The process of decomposition of the synthesized

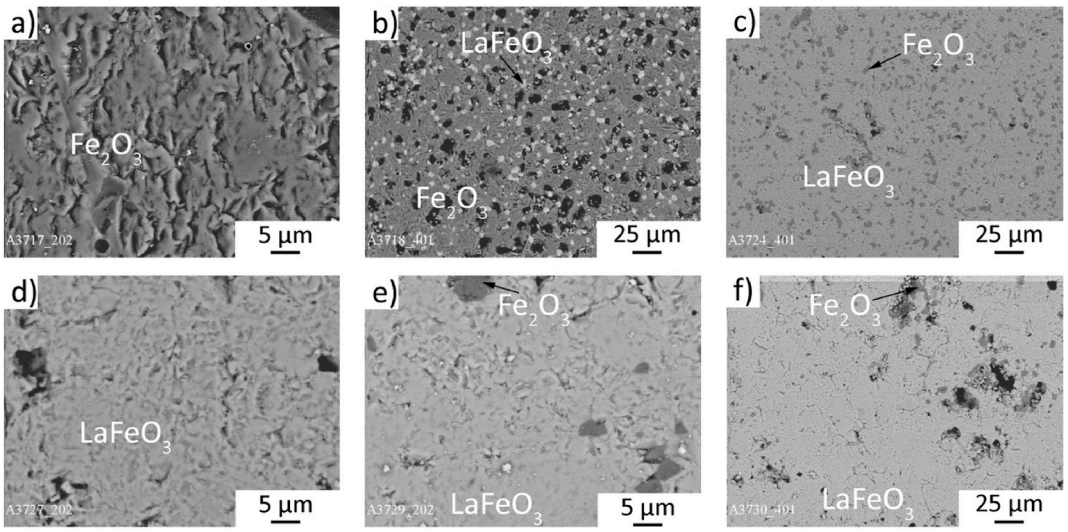


**Fig. 2.** – SEM microstructures of the samples in the definite field of compositions of the system $La_2O_3$–$Fe_2O_3$ heat-treated at 1300 °C: *a* – 0 mol % $La_2O_3$-100 mol % $Fe_2O_3$, *b* – 5 mol % $La_2O_3$-95 mol % $Fe_2O_3$; *c* – 45 mol % $La_2O_3$-55 mol % $Fe_2O_3$, *d* – 49 mol %$La_2O_3$-51 mol %$Fe_2O_3$, *e* – 50 mol % $La_2O_3$-50 mol % $Fe_2O_3$, *f* – 51 mol % $La_2O_3$-49 mol % $Fe_2O_3$.

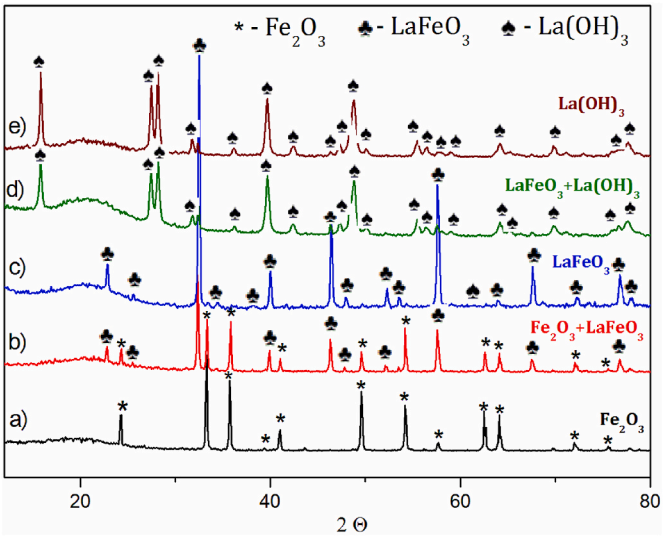


**Fig. 3.** – XRD patterns of the samples for the $La_2O_3$–$Fe_2O_3$ heat-treated at 1300 °C: *a* – 0 mol % $La_2O_3$-100 mol % $Fe_2O_3$; *b* – 15 mol % $La_2O_3$-85 mol % $Fe_2O_3$; *c* – 49 mol % $La_2O_3$-51 mol % $Fe_2O_3$; *d* – 95 mol % $La_2O_3$-5 mol % $Fe_2O_3$; *e* – 100 mol % $La_2O_3$-0 mol % $Fe_2O_3$.

precursors is completed at temperatures of ~800°C, depending on their synthesis, phase composition, amorphous or amorphous crystalline, specific surface area, and priority size of mesopores. The absence of extremes from 670 to 1000 °C indicates that the reaction is complete and no phase transitions occur in the sample.

### 3.3. Structural properties of nanopowders based on the perovskite phase obtained by various methods

Fig. 6 presents XRD of powders obtained by different methods. The precursors are amorphous because they have a broad, blurred peak (halo) at 18–28°. Only one phase is present at all samples in the 800°C, the presence of other peaks corresponding to La, $La_2O_3$, $Fe_2O_3$, or any additional phases are not observed (Table 3). The main peaks belong to the planes (101), (111), (121), (220), (202), (240), (141), (242), (204).

Analysis of the IR spectra of the samples indicated the presence of intense absorption bands in the frequency range $\nu$~ 800–450 $cm^{-1}$, which characterize M – O vibrations, where M = La, Fe (Fig. 7). The absorption bands in the frequency range $\nu$ ~1600-1300 $cm^{-1}$ characterize the vibrations of carbonate and nitrate ions in different monodentate and bidentate coordination. Two peaks with frequencies $\nu$~463 and 550 $cm^{-1}$ indicate the formation of $LaFeO_3$. Weak absorption band $\nu$~1630 $cm^{-1}$ characterize deformational OH vibrations. In addition, the IR spectrum of the $LaFeO_3$(II) sample has a distinct band with a frequency of $\nu$ ~677 $cm^{-1}$, which can be attributed to both La-O and Fe-O vibrations in the remaining unreacted precursor. A wide absorption band with a frequency of $\nu$~3450 $cm^{-1}$ characterizes valence OH vibrations, and a weak absorption band $\nu$~1630 $cm^{-1}$ characterizes deformational [29]. In addition, lanthanides have a strong tendency to absorb water and carbon dioxide, so the absorption peaks of OH, CO, and NO groups can be seen in the infrared spectra of these compounds.

### 3.4. Investigation of the morphology and fine structure of $LaFeO_3$ obtained by different methods

The EDS spectra during the TEM study for $LaFeO_3$(I) and $LaFeO_3$(II) synthesized by two methods have three elements: La, Fe, and O (Table 4). The atomic percentages (at %) of La and Fe for $LaFeO_3$(I) and $LaFeO_3$(II) are 15.6 and 15.8 and 16.0 and 17.3, respectively. Regardless of the production technology the powders had a conglomerate form, Fig. 8a and Fig. 9a. A more detailed analysis at high magnification revealed particles whose size does not exceed 100 nm, Figs. 8b–Fig. 9b. The morphology of powder particles primarily depends on the method of material synthesis. Larger particles consist of several nuclei between which internal boundaries are observed, that is, the formation of particles takes place in competition between the processes of nucleation and growth of nuclei

The diffraction pattern, SAED, from polycrystalline $LaFeO_3$(I) is fully consistent with the theoretical calculation (ICDD card No. 88–641) with the presence of all diffraction reflections, Fig. 8 d. A similar situation was observed during diffraction from a single crystal $LaFeO_3$ particle synthesized by method II, Fig. 9 d. The HRTEM image (Fig. 8e and 9c) shows lattice bands with d = 0.279 nm and d = 0.290 nm, which corresponds to the crystallographic plane (121) of $LaFeO_3$.

Therefore, the synthesized materials fully corresponded to the $LaFeO_3$ phase both from the chemical analysis and from the diffraction. According to the Pechini method, more conglomerated particles can be obtained, leading to a diffraction pattern for a polycrystalline material. At the same time, synthesis by method II allows to obtain more homogeneous non-conglomerated monocrystalline particles of regular shape (L/S~1.25).

**Table 2**
Composition of the phases in the samples, annealed at 1300 °C in air (EDX data).

| Chemical composition (mol %) | | Elemental composition (at %) | | | |
|---|---|---|---|---|---|
| $La_2O_3$ | $Fe_2O_3$ | Spectrum | O | La | Fe |
| 50 | 50 | S1 | 28.3 | 17.5 | 19.4 |
| | | S2 | 32.2 | 0.6 | 41.7 |
| 51 | 49 | S3 | 36.2 | 27.0 | 30.1 |
| | | S4 | 42.6 | 0.8 | 52.7 |

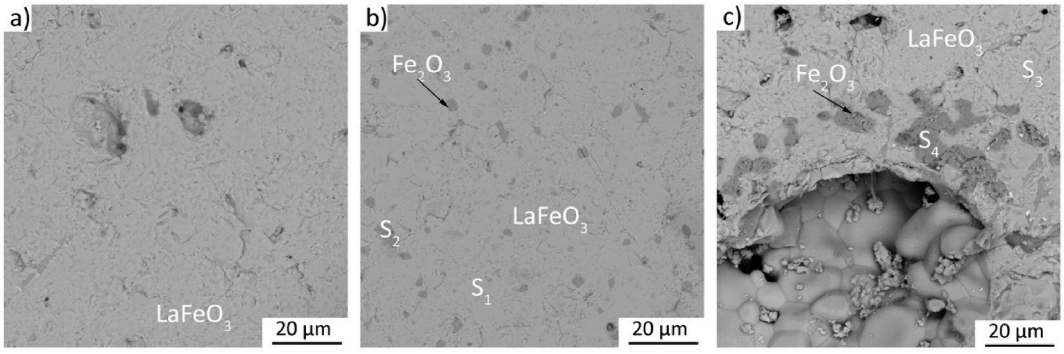


**Fig. 4.** – SEM microstructures of the samples heat-treated at 1300 °C in the system $La_2O_3$–$Fe_2O_3$: a) 49 mol% $La_2O_3$–51 mol% $Fe_2O_3$, b) 50 mol % $La_2O_3$ – 50 mol % $Fe_2O_3$, c) 51 mol % $La_2O_3$ – 49 mol % $Fe_2O_3$.

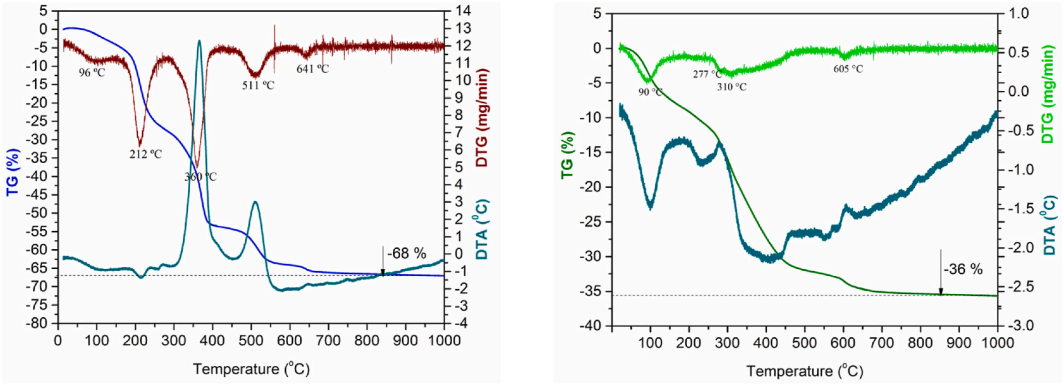


**Fig. 5.** – Thermal analysis curves of precursor powders: a) Pechini method (I), b) heterogeneous deposition method (II).

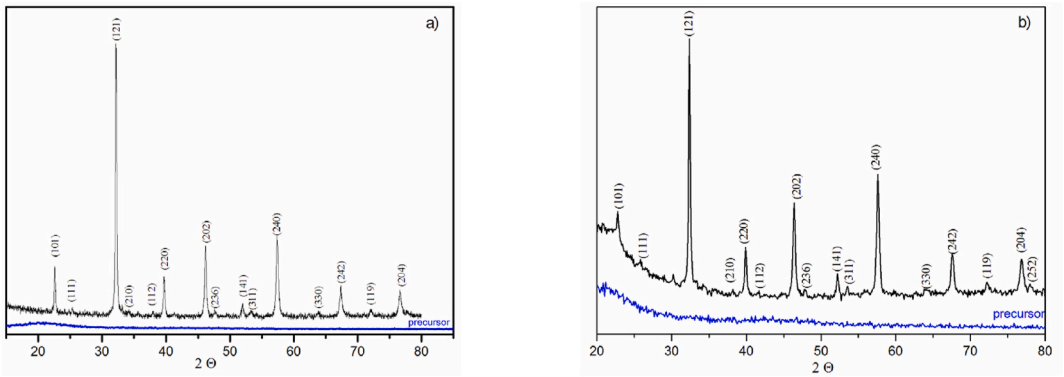


**Fig. 6.** – XRD of nanopowders based on the perovskite phase: a) Pechini method (I), b) heterogeneous deposition method (II).

**Table 3**
– Structural properties of nanopowders based on the perovskite phase.

| Sample | Lattice parameters of the phases, nm | | |
|---|---|---|---|
| | *a* | *b* | *c* |
| $LaFeO_3$(I) | 0.552 | 0.785 | 0.555 |
| $LaFeO_3$(II) | 0.554 | 0.784 | 0.553 |

### 3.5. *Investigation of magnetic properties of $LaFeO_3$ nanopowders*

The H vs M curve of materials synthesized, and different methods and temperature are depicted on Figs. 10 and 11. The magnetic properties of these materials are associated with the presence of $Fe^{3+}$ ions since the lanthanum ion does not exhibit them. A Dzyaloshinskii-Moriya (DM) interaction in containing ion iron materials induces a canting of the spin lattice, leading to a weak ferromagnetic response.

**Table 4**
– Composition of the phases in the samples (EDS data).

| Chemical composition (mol %) | | Elemental composition (at %) | | | |
|---|---|---|---|---|---|
| $La_2O_3$ | $Fe_2O_3$ | | O | La | Fe |
| 49 | 51 | $LaFeO_3$(I) | 68.65 | 15.58 | 15.76 |
| 49 | 51 | $LaFeO_3$(II) | 66.25 | 16.00 | 17.13 |

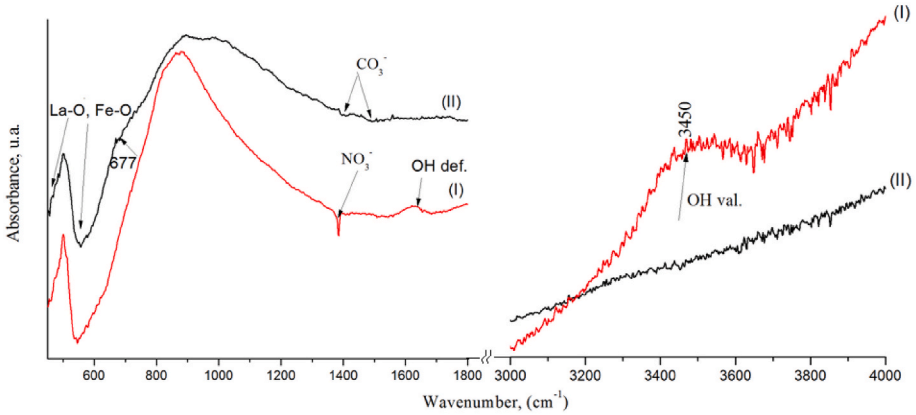


**Fig. 7.** – Infrared spectra of samples $LaFeO_3$(I) i $LaFeO_3$(II).

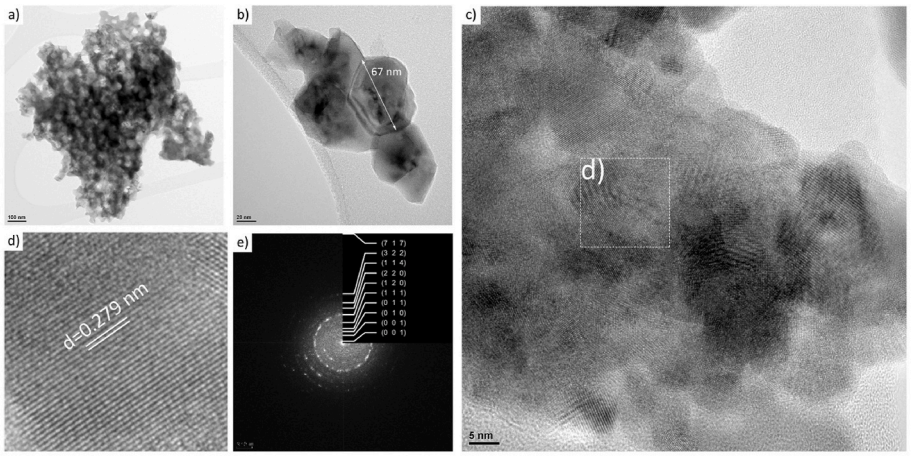


**Fig. 8.** – TEM of $LaFeO_3$ synthesized by I method: (a-c,e) and SAED of particles (e).

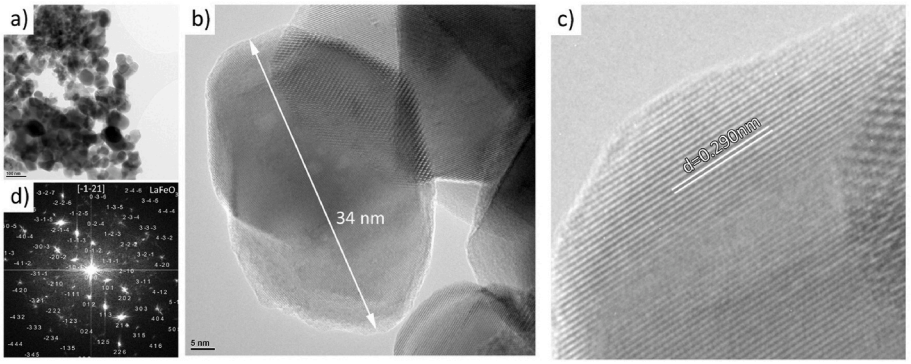


**Fig. 9.** – TEM of $LaFeO_3$ synthesized by II method: (a–c) and SAED of single crystal (d).

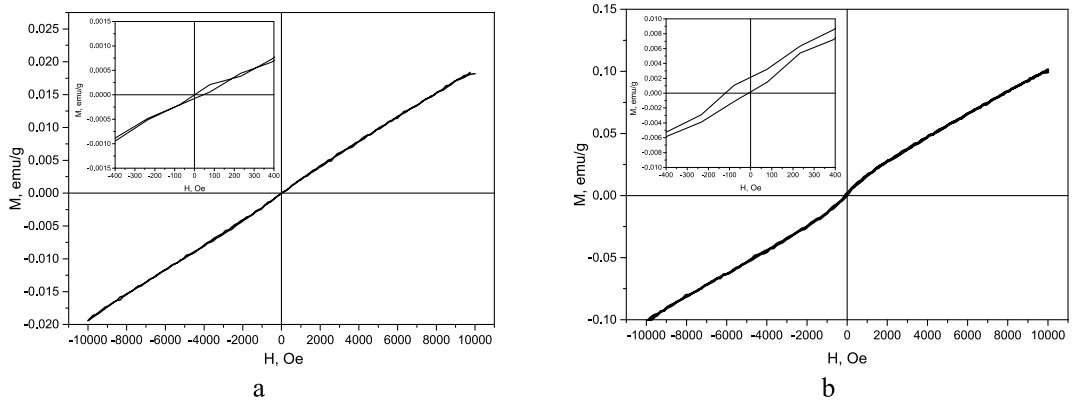


**Fig. 10.** – Magnetic properties of $LaFeO_3$ (I) synthetized at 800 °C (a) and $LaFeO_3$ (II) (b) synthetized at 800 °C.

The magnetic transition temperature in materials is closely related to the ionic radius of the A site element where the transition temperature increases with the ionic radius. The interaction of iron and oxygen ions induces a pattern of ferromagnets on the particle's surface due to spin disordering, while the core of antiferromagnets is induced due to spin ordering. This behavior indicates that the ratio of the volume fraction of disordered spins to the ordered spin of Fe3 þ ions increases with decreasing particle size as well as large surface area, leading to greater magnetic interaction [30]. Materials obtained at a temperature of 800 °C retained the structure of nanopowders. Therefore, the $LaFeO_3$ has strong antiferromagnetic properties, Fig. 10. The difference between $LaFeO_3$(I) and $LaFeO_3$(II) is the higher coercivity, Fig. 10a and b. We associate it with different magnetically disordered of the surface layer in the particle size. The same situation was observed in $La_{0.67}Sr_{0.33}MnO_3$ material [31]. On the other hand, the higher value of the coercivity for the small nanoparticles indicates that the presence of a nonmagnetic layer with random spin orientation and the thickness of this layer increases with the decrease in particle size.

Increasing the temperature of annealing up to 1300 °C the ferrimagnetic properties increases, Fig. 11. Because during the annealing at 1300 °C process of densification was occurred. It leads to formation of dense materials. Dense materials had domain and could be magnetized. The difference in magnetic properties remained because the during sintering the nanoparticle growth with different speed.

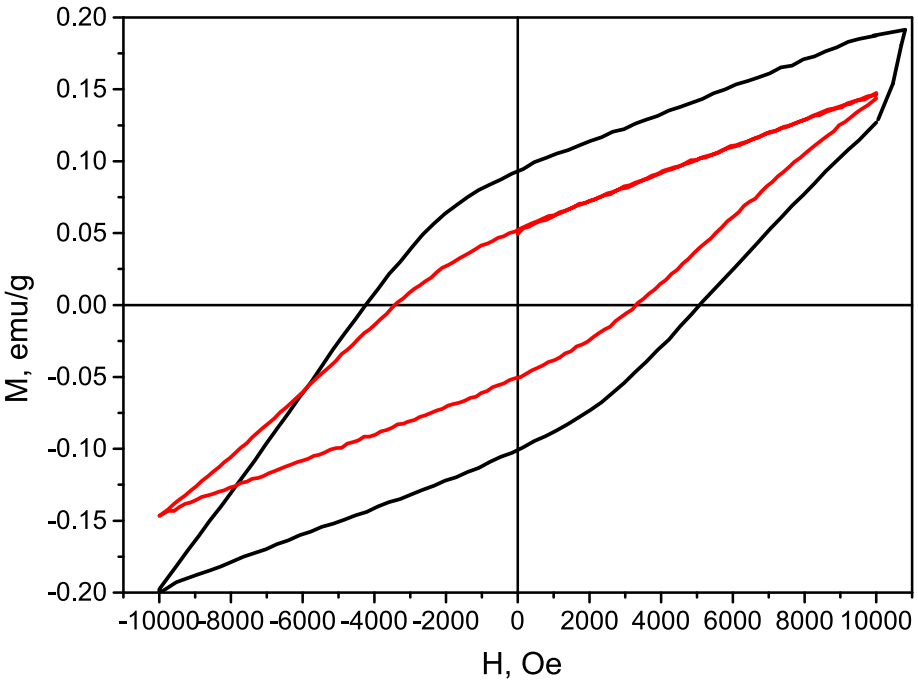


**Fig. 11.** – Magnetic properties of $LaFeO_3$ (I) synthetized at 1300 °C (black line) and $LaFeO_3$ (II) synthetized at 1300 °C (red line) The bulk $LaFeO_3$ is an antiferromagnet, the studied $LaFeO_3$ sample exhibited a weak ferromagnetic signal for materials obtained at 800°C and strong ferromagnetic signal at 1300°C.

It is known that $LaFeO_3$ structure has $FeO_6$ octahedra are corner linked, forming a three-dimensional polyhedral network. The $La^{3+}$ ions are located in the cavities in $FeO_6$ octahedral units. Therefore, there is no magnetic interaction between $La^{3+}$ and $Fe^{3+}$ within the structure. Furthermore, the nanocrystalline structure of the sample can result in significant surface spin disorder. The significant increase in the saturation magnetization may arise from the double-exchange interaction between $Fe^{4+}$ and $Fe^{3+}$ ions, which is induced by magnetic $Fe^{3+}$ ion doping of the parent compound.

The pure $La_2O_3$ has coercivity of 30 kA/m [33]. Change the structure to $LaFeO_3$ led to increase the coercivity to 40 and 32 kA/m for $LaFeO_3$(I) (1300°C) and $LaFeO_3$(II) (1300 °C), respectively (Table 5).

Therefore, the use of the Pechini method or heterogeneous deposition methods with annealing at 1300 °C allows to obtain $LaFeO_3$ with higher coercivity and magnetization than already known composites.

## 4. Conclusions

The phase relations in the $La_2O_3$–$Fe_2O_3$ system at 1300 °C were studied in the whole concentration range by X-ray diffraction (XRD) and scanning electron microscopy (SEM). The samples were prepared with a concentration step of 1–5 mol %. The isothermal cross-sections of the $La_2O_3$–$Fe_2O_3$ phase diagram at 1300 °C are characterized by the presence of three single-phase (A-$La_2O_3$, $LaFeO_3$, $Fe_2O_3$), two two-phase (A-$La_2O_3$+$LaFeO_3$, $LaFeO_3$+$Fe_2O_3$) regions. The composition corresponding to the perovskite phase is 49 mol % $La_2O_3$-51 mol % $Fe_2O_3$. Nanocomposites based on the perovskite phase ($LaFeO_3$) were obtained by the Pechini method and heterogeneous precipitation from nitrate solutions. Nanopowders are single-phase with a perovskite structure. Two IR peaks with frequencies $\nu$ ~463 and 550 $cm^{-1}$ indicate the formation of $LaFeO_3$ too. The synthesized materials fully correspond to the $LaFeO_3$ phase both from the point of view of chemical analysis and from the point of view of diffraction. According to the Pechini method ($LaFeO_3$(I)) more conglomerated particles can be obtained, leading to a diffraction pattern for a polycrystalline material. At the same time, synthesis by heterogeneous deposition ($LaFeO_3$(II)) allows for obtaining more homogeneous non-conglomerated particles with more round shape (L/S~1.25). The studied $LaFeO_3$ sample exhibited a weak ferromagnetic signal for materials obtained at 800°C and strong ferromagnetic signal at 1300 °C. The coercivity of $LaFeO_3$(I) (1300 °C) and $LaFeO_3$(II) (1300 °C) are 40 and 32 kA/m, respectively. The specific magnetization of $LaFeO_3$(I) (1300 °C) and $LaFeO_3$(II) (1300 °C) are 0.2 and 0.15 kA/m, respectively.

**Table 5**
– Comparison the magnetic properties of $LaFeO_3$.

| Composition | Methods of synthesis | M, emu/g | Coercivity, kA/m | Ref |
|---|---|---|---|---|
| $La_2O_3$ | Decompaction of polymer | 0.03 | – | [33] |
| $LaFeO_3$ | Calcination | – | 30 | [32] |
| $LaFeO_3$(I) (1300 °C) | Pechini method | 0.2 | 40 | Present work |
| $LaFeO_3$(II) (1300 °C) | Heterogeneous deposition | 0.15 | 32 | Present work |
| $La_{0.5}Fe_{0.5}O_3$ | Calcination | – | 6.8 | [32] |
| $LaFeO_3$ | Calcintion with polymet at 750 °C | 0.1 | – | [34] |
| $LaFeO_3$ | Calcintion with polymet at 1050 °C | 0.09 | – | [34] |
| $Fe_3O_4$ | Decomposition of $FeCl_3{\cdot}6H_2O$, NaAc | 20 | 62 | [35] |

## CRediT authorship contribution statement

**O.V. Chudinovych:** Investigation, Methodology, Visualization, Writing – original draft preparation. **D.V. Vedel:** Investigation, Visualization, Writing – review & editing. **O.O. Stasyuk:** Investigation. **T.V. Tomila:** Investigation. **M.H. Aguirre:** Investigation, Writing – review & editing.

## Declaration of competing interest

The authors declare that they have no known competing financialinterestsor personal relationships that could have appeared to influence the work reported in this paper.

## Data availability

The authors are unable or have chosen not to specify which data has been used.

## Acknoledgement

We acknowledge the financial support of the European Commission through the project H2020-MSCA-RISE 2020 MELON (Grant No. 872631). The authors would like to acknowledge the access to the equipment of "Servicio General de Apoyo a la Investigación (SAI), Universidad de Zaragoza".

## References

[1] S.F. Wang, J. Zhang, D.W. Luo, F. Gu, D.Y. Tang, Z.L. Dong, W.X. Que, T.S. Zhang, S. Li, L.B. Kong, Transparent ceramics: processing, materials and applications, Prog. Solid State Chem. 41 (2013) 20–54, https://doi.org/10.1016/j.progsolidstchem.2012.12.002.

[2] M. Boniecki, Z. Librant, A. Wajler, W. Wesolowski, Fracture toughness, strength and creep of transparent ceramics at high temperature, Ceram. Int. 38 (2012) 4517, https://doi.org/10.1016/j.ceramint.2012.02.028.

[3] B.S. Chen, Y. Wu, New opportunities for transparent ceramics, Am. Ceram. Soc. Bull. 2 (2013) 32–37.

[4] N. Lakshminarasimhan, U.V. Varadaraju, Luminescent host lattices, $LaInO_3$ and $LaGaO_3$ reinvestigation of luminescence of metal ions, Mater. Res. Bull. 41 (2006) 724–731, https://doi.org/10.1016/j.materresbull.2005.10.010.

[5] M. Ivanov, E. Kalinina, Yu Kopylov, V. Kravchenko, Highly transparent Yb-doped $(La_xY_{1-x})_2O_3$ ceramics prepared through colloidal methods of nanoparticles compaction, J. Eur. Ceram. Soc. 36 (16) (2016) 4251, https://doi.org/10.1016/j.jeurceramsoc.2016.06.013.

[6] A. Jun, S. Yoichi, T. Takunori, J. Akiyama, Laser ceramics with rare-earth-doped anisotropic materials, Opt Lett. 35 (21) (2010) 3598, https://doi.org/10.1364/OL.35.003598.

[7] L. Zehua, S. Li, Y. Huang, L. Wang, Y. Yao, T. Long, X. Yao, X. Liu, Z. Huang, Composite ceramic with high saturation input powder in solid-state laser lighting: microstructure, properties, and luminous emittances, Ceram. Int. 44 (16) (2018) 20232, https://doi.org/10.1016/j.ceramint.2018.08.008.

[8] O.V. Chudinovych, D.V. Myroniuk, L.A. Myroniuk, O.V. Shyrokov, I.M. Danylenko, Structure, optical properties and photocatalytic activity of undoped, $Nd_2O_3$-doped ZnO nanocomposites, Functional Materials 30 (2023) 1–7, https://doi.org/10.15407/fm30.02.1.

[9] O.V. Chudinovych, D.V. Myroniuk, L.A. Myroniuk, O.I. Olifan, O.V. Shyrokov, I. M. Danylenko Structure, Optical properties and photocatalytic activity of undoped, $Y_2O_3$-doped ZnO nanocomposites, Journal of chemistry and technologies 32 (1) (2024) 17–29, https://doi.org/10.15421/jchemtech.v32i1.286092.

[10] V. Rizos, E. Righetti, A. Kassab, Developing a supply chain for recycled rare earth permanent magnets in the, EU (2022) 57.

[11] M. Theingi, K. Thi Tu, N. Aung, Preparation, characterization and optical property of $LaFeO_3$ nanoparticles via sol-gel combustion method, SciMedicine Journal 1 (3) (2019), https://doi.org/10.28991/SciMedJ-2019-0103-5.

[12] H. Chai, Y. Li, Y. Luo, M. Debliquy, C. Zhang, Investigation on isopropanol sensing properties of $LnFeO_3$(Ln = Nd, Dy, Er) perovskite materials synthesized by microwave-assisted hydrothermal method, Appl. Surf. Sci. 601 (2022) 154292, https://doi.org/10.1016/j.apsusc.2022.154292.

[13] Zhiqiang Zhoua, Li Guob, Haixia Yanga, Qiang Liua, Feng Ye, Hydrothermal synthesis and magnetic properties of multiferroic rare-earth orthoferrites, J. Alloys Compd. 583 (2014) 21–31, https://doi.org/10.1016/j.jallcom.2013.08.129.

[14] I.P. Parkin, A.V. Komarov, Q. Fang, Alternative solid state routes to mixed metal oxides ($LnCrO_3$, $LnFeO_3$), Polyhedron 15 (18) (1996) 3117–3121, https://doi.org/10.1016/0277-5387(95)00576-5.

[15] S. Thirumalairajan, K. Girija, N. Hebalkar, D. Mangalaraj, Shape evolution of perovskite $LaFeO_3$ nanostructures: a systematic investigation of growth mechanism, properties and morphology dependent photocatalytic activities, The Royal Society of Chemistry 3 (2013) 7549–7561, https://doi.org/10.1039/c3ra00006k.

[16] N.A. Tien, H. Thi Kim Hoang, V.O. Mittova, Tran T. To Nga, N. Thi Truc Linh, I. Y. Mittova, E.V. Tomina, T.D. Trinh, L.T. Thanh Thuy, T.S. Cam, Structural, optical, and magnetic properties of *o*-$TbFeO_3$ nanomaterials synthesized by the co-precipitation method, ChemistrySelect 8 (2023) 202303386, https://doi.org/10.1002/slct.202303386.

[17] N.A. Tien, C.T. Son, V.O. Mittova, I.Y. Mittova, E.V. Tomina, T. Chi Hien, B. X. Vuong, Influenceof synthetic conditions on the crystal structure, optical and magnetic properties of o-$EuFeO_3$ nanoparticles, Coatings 13 (2023) 1082, https://doi.org/10.3390/coatings13061082.

[18] S. Mathur, M. Veith, R. Rapalaviciute, H. Shen, G.F. Goya, W.L. Martins Filho, T. S. Berquo, Molecule derived synthesis of nanocrystalline $YFeO_3$ and investigations on its weak ferromagnetic behavior, Chem. Mater. 16 (2004) 1906–1913, https://doi.org/10.1021/cm0311729.

[19] X. Niu, H. Li, G. Liu, Preparation, characterization and photocatalytic properties of $REFeO_3$ (RE=Sm, Eu, Gd), J. Mol. Catal. Chem. 232 (2005) 89–93, https://doi.org/10.1016/j.molcata.2005.01.022.

[20] S. Phokha, S. Pinitsoontorn, S. Maensiri, S. Rujirawat, Structure, optical and magnetic properties of $LaFeO_3$ nanoparticles prepared by polymerized complexmethod, J. Sol. Gel Sci. 71 (2) (2014) 333–341, https://doi.org/10.1007/s10971-014-3383-8.

[21] M. Pidburtnyi, B. Zanca, C. Coppex, S. Jimenez-Villegas, V. Thangadura, A review on perovskite-type $LaFeO_3$ based electrodes for $CO_2$ reduction in solid oxide electrolysis cells: current understanding of Structure−Functional property relationships, Chem. Mater. 33 (2021) 4249–4268, https://doi.org/10.1021/acs.chemmater.1c00771.

[22] L.C. Sonia Pinho, J.S. Amaral, A. Wattiaux, M. Duttine, M.-H. Delville, Synthesis and characterization of rare-earth orthoferrite $LnFeO_3$ nanoparticles for bioimaging, Eur. J. Inorg. Chem. 31 (2018) 3570–3578, https://doi.org/10.1002/ejic.201800468.

[23] A.T. Nguyen, N.T. Nguyen, I.Y. Mittova, N.S. Perov, V.O. Mittova, T.C. Chuong Hoang, V. Nguyen, V.H. Nguyen, V. Pham, X.V. Bui, Crystal structure, optical and magnetic properties of $PrFeO_3$ nanoparticles prepared by modified co-precipitation method, Processing and Application of Ceramics 14 (4) (2020) 355–361, https://doi.org/10.2298/PAC2004355N.

[24] O.V. Chudinovych, O.R. Andrievskaya, J.D. Bogatyryova, V.V. Kovylyaev, O. I. Bykov, Phase equilibria in the $La_2O_3$-$Y_2O_3$-$Nd_2O_3$ system at 1500 °C, J. Eur. Ceram. Soc. 41 (2021) 6606–6616, https://doi.org/10.1016/j.jeurceramsoc.2021.06.017.

[25] O.V. Chudinovych, O.I. Bykov, A.V. Sameliuk, Interaction of lanthanum, lutetium, and ytterbium oxides at 1600 °C, Powder Metall. Met Ceram. 60 (5–6) (2021) 337–345, https://doi.org/10.1007/s11106-021-00248-8;

[25] O.V. Chudinovych, O.V. Shyrokov, A.V. Sameliuk, Phase equilibria in the $La_2O_3$-$Lu_2O_3$-$Er_2O_3$ system at 1500 and 1600 °C, Journal of chemistry and technologies 31 (1) (2023) 51–60, https://doi.org/10.2139/ssrn.4282465.

[26] O.V. Shyrokov, O.V. Chudinovych, T.F. Lobunets, A.V. Ragulya, Formation of complex phase $LaLuO_3$:$Yb^{3+}$ nanopowders with perovskite type structures, Functional materials 28 (2) (2021) 366–374, https://doi.org/10.15407/FM28.02.366.

[27] Y. Goto, T. Kitamura, T. Takada, S. Kachi, Phase Diagram of the System $La_2O_3$-$Fe_2O_3$, Annual Meeting of Japan Society of Powder Metallurgy, Tokyo, 1960, pp. 227–231.

[28] V.L. Moruzzi, M.W. Shafer, Phase equilibria in the system $La_2O_3$-iron oxide in air, J. Am. Ceram. Soc. 43 (7) (1960).

[29] N. Sivakumar, P. Nagaraju, A. Alsalme, A. Alghamdi, R. Jayavel, Enhance delectrochemical performance of lanthanum ferritedecorated reducedgraphene oxidenanocomposite electrodes preparedby insitumicrowave irradiation for energy storage applications, Int. J. Energy Res. (2020) 1–11. https://doi:10.1002/er.6146.

[30] S. Phokha, S. Pinitsoontorn, S. Rujirawat, S. Maensiri, Polymer pyrolysis synthesis and magnetic properties of $LaFeO_3$ nanoparticles, Physica B 476 (2015) 55–60, https://doi.org/10.1016/j.physb.2015.07.021.

[31] Yu Zhou, X. Zhu, S. Li, Effect of particle size on electric and magnetic transport properties of $La_{0.67}Sr_{0.33}MnO_3$ coatings, Phys. Chem. Chem. Phys. (2013), https://doi.org/10.1039/C5CP04477D.

[32] C.G. Ünlü, M.B. Kaynar, T. Simsek, A. Tekgül, B. Kalkan, S. Ozcan, Structure and magnetic properties of $(La_{1-x}Fe_x)FeO_3$ (x = 0, 0.25, 0.50) perovskite, J. Alloys Compd. 784 (2019) 1198–1204. https://doi:10.1016/j.jallcom.2019.01.047.

[33] Z. Razmara, Lanthanum(III) complex as ferromagnetic supraprecursor for preparation of $La_2O_3$ nanoparticles by thermal decomposition method, Res. Chem. Intermed. 5 (2019) 2887–2901, https://doi.org/10.1007/s11164-019-03768-6.

[34] S. Phokha, S. Pinitsoontorn, S. Maensiri, S. Rujirawat, Structure, optical and magnetic properties of $LaFeO_3$ nanoparticles prepared by polymerized complex method, J. Sol. Gel Sci. Technol. 71 (2) (2014) 333–341, https://doi.org/10.1007/s10971-014-3383.

[35] M.D. Nguyen, H.-V. Tran, S. Xu, T. Randall Lee, $Fe_3O_4$ nanoparticles: structures, synthesis, magnetic properties, surface functionalization, and emerging applications, Appl. Sci. 11 (23) (2021) 11301, https://doi.org/10.3390/app112311301.